

One-dimensional fluid model for an rf methane plasma of interest in deposition of diamond-like carbon layers

D. Herrebout, A. Bogaerts,^{a)} M. Yan, and R. Gijbels

Department of Chemistry, University of Antwerp, Universiteitsplein 1, 2610 Wilrijk, Belgium

W. Goedheer

FOM-Institute for Plasma Physics RIJNHUIZEN, P.O. Box 1207, 3430 BE Nieuwegein, the Netherlands

E. Dekempeneer

Vlaamse Instelling voor Technologisch Onderzoek (VITO), Boeretang 200, 2400 Mol, Belgium

(Received 21 December 2000; accepted for publication 12 April 2001)

A one-dimensional (1D) model for a methane rf plasma consisting of 20 species (neutrals, radicals, ions, and electrons) is presented. The equations solved are the particle balances, assuming a drift-diffusion approximation for the fluxes, and the electron energy balance equation. The self-consistent electric field is obtained from the simultaneous solution of Poisson's equation. The electron-neutral collision rates are expressed as a function of the average electron energy. These expressions are obtained from the solution of the Boltzmann equation using the Lorentz approximation. The results presented in this article are limited to the alpha regime, hence no secondary electrons are considered. In total, 27 electron reactions (vibrational excitation, dissociation, and ionization) have been included in the model, as well as seven ion-neutral reactions and 12 neutral-neutral reactions. The 1D fluid model yields, among others, information about the densities of the different species in the plasma. It is found that in a methane plasma C_2H_6 , C_3H_8 , C_2H_4 , and C_2H_2 are also present at high densities, together with CH_4 and H_2 (inlet gases). The main radical in the plasma is CH_3 . At low pressure (e.g., 0.14 Torr) the most important ion is found to be CH_5^+ , at higher pressure (e.g., 0.5 Torr) $C_2H_5^+$ becomes the dominant ion. © 2001 American Institute of Physics. [DOI: 10.1063/1.1378059]

I. INTRODUCTION

Plasma assisted chemical vapor deposition (PACVD) reactors are frequently used to deposit amorphous carbon (α -C:H) layers on materials.^{1,2} These layers, also called diamond-like carbon layers, can be deposited on a variety of substrates by PACVD using different kinds of plasmas, i.e., a microwave plasma,³ an electron cyclotron resonance plasma,⁴ an inductively coupled plasma,⁵ or a capacitively coupled rf plasma.⁶ In order to improve the deposition process, plasma modeling can be of great use to predict the composition of the plasma and to optimize the plasma parameters (pressure, power, gas flow, and gas mixture). In recent years, a number of methane plasma models have been published.^{1,4,6-13} Tachibana *et al.*⁶ developed a plasma model where all the particle balance equations are solved interactively assuming steady state. The other models can be subdivided in the way they treat the electron kinetics. In some models,^{7,8} constant electron reaction rate coefficients were used, whereas the plasma model described in Ref. 9 used the electron reaction rate coefficients as fitting parameters. In other cases, a Maxwellian⁴ or a Druyvesteynlike^{10,11} electron energy distribution function was assumed for the calculation of the electron reaction rate coefficients. In Ref. 1, a fluid model (comparable with the fluid model we present here) was developed which was coupled with a Boltzmann equa-

tion solver for a dc field calculation of the electron energy distribution function (EEDF). As input for this fluid model, swarm data were used. In the present work we have developed a one-dimensional (1D) fluid model for a methane plasma (consisting of 20 species) that is based on the first three moments of the Boltzmann equation. The EEDF is obtained from the Boltzmann equation using the Lorentz approximation. With this method, the electron reaction rate coefficients are obtained for every electron reaction, as a function of average electron energy (0–20 eV). This way of handling the electron kinetics has already proven to be successful in the past¹⁴ for the simulation of silane plasmas. While some models^{6,9,10,13} described above make use of total cross sections assuming certain accompanying fragmentation patterns for the different species formed in the electron reaction, we tried to use as much as possible “partial” cross sections (i.e., individual cross sections for every reaction). In contrast to most of the models described above, we included two or more vibrational excitations for every nonradical neutral (C_2H_6 , C_3H_8 , C_2H_4 , C_2H_2 , CH_4 , and H_2). These reactions cannot be neglected because a considerable fraction of the electron energy is lost in the vibrational excitation reactions. The same result has been found for silane plasmas.¹⁴ Including these vibrational excitation reactions yields a more realistic EEDF, which implies a more realistic calculation of the production and loss terms for the different species described in the model. In the methane rf plasma model we present in this article, the following reactions are included:

^{a)}Electronic mail: bogaerts@uia.ua.ac.be

reactions between neutral species (neutral–neutral reactions), ion–neutral reactions, and electron–neutral reactions. The electron reactions can be divided into three categories: vibrational excitation, dissociation, and ionization. Electronic excitation is assumed to lead to dissociation and is therefore implicitly taken into account (see Sec. II B 1 below).

In Sec. II, the model is described. A detailed overview of all the reactions incorporated in the model is given, together with a calculation of the transport coefficients necessary for the model. A brief description of the boundary conditions for the different species described in the model is also given. In Sec. III, the results of the model are presented. These results are compared with experimental and calculated results found in the literature. Further, simulations were carried out for a range of parameter settings (power, pressure, gas flow, gas flow mixture) to investigate the effect of these parameters. Finally, the conclusions are given in Sec. IV.

II. DESCRIPTION OF THE MODEL

A. General description of the fluid model

The fluid model used in this work was originally developed by Nienhuis *et al.*^{14,15} for the simulation of silane rf discharges. This self-consistent 1D fluid model consists of the balance equations for the densities of the various species in the plasma (electrons, positive and negative ions, radicals and background neutrals). The gas inlet and pumping are incorporated into the model by means of additional source and sink terms in the density balance equations of the different species. The energy balance equation for the electrons is also included. For the ions, no energy balance equation is considered because the ion energy is assumed to be equal to the neutral gas thermal energy. The fluxes of the neutral and ionic species are calculated in the model by the drift-diffusion approximation: the diffusion term describes the transport of species due to the density gradient, while the drift term determines the transport of the charged species under the influence of the electric field. Because the ions cannot follow the actual electric field, an effective electric field is taken into account. All the equations mentioned above are coupled with the Poisson equation, to obtain the electric field. (See Ref. 14 for a more detailed description of the equations.)

All simulations were carried out for a small capacitively coupled rf PACVD reactor with a distance of 3 cm between the two electrodes. One electrode is electrically grounded while the other is connected to an rf (13.56 MHz) power supply. The 1D model gives information about the densities of the radical and the ionic species as a function of distance from the electrodes. The densities of the nonradical neutrals are assumed to be homogeneously distributed between the two electrodes and will be referred to as background neutrals in this article.

The source terms for the density balance equations are given by the electron reactions, the ion–neutral reactions, and the neutral–neutral reactions (see below). The electron reactions (ionization, dissociation, vibrational excitation) depend strongly on the electron energy distribution function. Before starting the fluid simulation, the EEDF is obtained for

a large number of electric field values from the Boltzmann equation, using the two-term expansion, for a given background gas density and composition. The distribution functions obtained in this way are used to construct a “look-up” table (i.e., for every value of the electric field, both the average electron energy and the various reaction rate coefficients are calculated from the EEDF, and this leads to a look-up table (reaction rate coefficients as a function of average electron energy) for every electron reaction)

The latter can be used afterwards to compute the source terms (i.e., the electron reaction rates) in the fluid model. Consequently, in the fluid model, the average electron energy is calculated as a function of space and time (from the electron energy balance equation) and the corresponding reaction rate coefficients, which are used as source terms in the density balance equations, can then be obtained from the look-up tables. The source term obtained from an electron reaction is given by the product kN_eN_{gas} , where k is the reaction rate coefficient, N_e the electron density, and N_{gas} the gas density of the gas which is involved in the reaction. The total source term for the density balance equation of a species is obtained by summation of the production and loss terms of all the reactions included. The reaction rate coefficients of the neutral–neutral reactions and the ion–neutral reactions, which are also required for the source terms in the density balance equations are assumed to be constant and are taken from the literature (see Secs. II B 2 and II B 3 below).

In the 1D rf model, no dc self-bias voltage is considered because both electrodes have the same size. The power input into the plasma is transferred to the charged species (electrons and ions) by ohmic heating. As discussed, the fluid model needs the electron reaction rate coefficients obtained from the Boltzmann equation as input, and on the other hand the latter requires the densities of the background gases calculated from the fluid code in order to construct the look-up tables. Hence, both parts (fluid part and EEDF part) are run iteratively until the changes in the density of the background gases are less than 10^{-4} . The convergence criterion of the fluid model is defined as the error between the discharge parameters (density of the species, potential, electron energy, electron density) at the beginning of two subsequent rf periods, and is typically set to 10^{-6} – 10^{-7} . The rf discharge operates in the alpha regime at the conditions under study, and therefore, secondary electrons could be neglected in the fluid model. It is worth mentioning that, at higher power, the capacitively coupled plasma is often operated in the gamma regime, where secondary electrons are important. It should be noted that, in such cases, the EEDF has a lower electron temperature and a higher energy tail than in the present case, which results in different electron-impact reaction rates and different radical compositions.

Compared to a 2D model,^{11,16} the 1D model has the great advantage of a reduction in computation time, while important information about the plasma characteristics and the densities of the species can still be obtained. Therefore, the 1D fluid model is very useful for a sensitivity study to investigate which reactions and species are the most important in the methane plasma. The results of this sensitivity study for a methane plasma are given in Sec. II B. The main

TABLE I. Different species taken into account in the methane plasma model, beside electrons.

Neutrals	Ions	Radicals
CH ₄ , H ₂	CH ₄ ⁺ , CH ₃ ⁺ , H ₂ ⁺	C ₂ H ₅ , CH ₃
C ₂ H ₆ , C ₃ H ₈	CH ₅ ⁺ , C ₂ H ₅ ⁺ , H ₃ ⁺	CH ₂ , CH
C ₂ H ₄ , C ₂ H ₂	C ₂ H ₄ ⁺ , C ₂ H ₂ ⁺	H

disadvantage of a 1D model is that no information is obtained about the fluxes of the species towards the electrodes as a function of the radial distance, hence, no information can be obtained about the uniformity of the deposited layer.

B. Fluid model applied to a methane/hydrogen plasma

A sensitivity analysis showed that the methane/hydrogen plasma can be modeled in a realistic way using 20 species. An overview of the species (electrons, ions, radicals, and background neutrals) taken into account in the model is given in Table I. First of all, the inlet gas (CH₄ or a mixture of CH₄/H₂) plays an important role in the plasma, and these gases are present in the plasma at high densities. It is found in the literature^{6,12} that higher order neutral molecules (C₂H₆, C₃H₈, C₂H₄, C₂H₂) are also present in the plasma at high densities; hence, these species are also included in our model. Although we have included for every nonradical neutral molecule two or more vibrational excitation reactions, these vibrationally excited species are not taken into account separately in order to limit the number of species in the model. Furthermore, eight ionic and five radical species are described in the model (see Table I). Although it is experimentally found¹⁷ that some other radical and ionic species (e.g., C₂H₃, C₃H₄, C₂H₃⁺, ...) are present in a methane plasma at lower densities, they are not considered in our model. Negative ions (mainly CH₂⁻ and H⁻) are not incorporated either, because it is found¹ that the negative ion density in a methane plasma is about one order of magnitude lower than the electron and positive ion densities. Hence, a CH₄ plasma has a strong electropositive character. This is in contrast to a SiH₄ plasma, where negative ions play a much more important role in the plasma (electronegative discharge).¹⁴

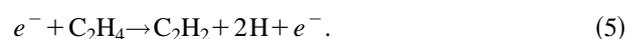
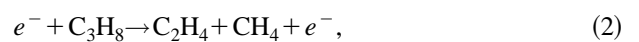
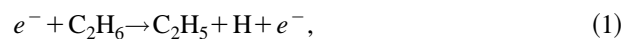
1. Electron impact collisions taken into account in the model

An overview of the electron impact reactions (i.e., ionization, dissociation, and vibrational excitation) taken into account in the model is given in Table II. Electronic excitation reactions were not included in the model because it is found in the literature that for methane,¹⁸ as well as for silane and disilane,¹⁹ all excited states of these molecules lead to dissociation. Hence, we have also assumed that the electron reactions causing electronically excited states for the higher order neutrals (C₂H₆, C₃H₈, C₂H₄, C₂H₂) lead to dissociation. Information about the cross sections of rotational excitation of the various nonradical neutral molecules is very difficult to find, but since rotational excitation clearly takes much less energy away from the electrons than vibrational excitation, it seems justified not to include rotational excita-

TABLE II. Electron reactions with molecules, taken into account in our model. The number of different vibrational excitation reactions is given between brackets. (vibr. exc. stands for vibrational excitation)

Reaction	Chemical reaction	Ref.
	CH ₄	
vibr. exc.	$e^- + \text{CH}_4 \rightarrow \text{CH}_4^* + e^-$ (2)	20
ionization	$e^- + \text{CH}_4 \rightarrow \text{CH}_4^+ + 2e^-$	20
ionization	$e^- + \text{CH}_4 \rightarrow \text{CH}_3^+ + \text{H} + 2e^-$	20
dissociation	$e^- + \text{CH}_4 \rightarrow \text{CH}_3 + \text{H} + e^-$	36
dissociation	$e^- + \text{CH}_4 \rightarrow \text{CH}_2 + 2\text{H} + e^-$	36
	H ₂	
vibr. exc.	$e^- + \text{H}_2 \rightarrow \text{H}_2^* + e^-$ (3)	24
dissociation	$e^- + \text{H}_2 \rightarrow 2\text{H} + e^-$	37
ionization	$e^- + \text{H}_2 \rightarrow \text{H}_2^+ + 2e^-$	38
	C ₂ H ₆	
vibr. exc.	$e^- + \text{C}_2\text{H}_6 \rightarrow \text{C}_2\text{H}_6^* + e^-$ (3)	21
ionization	$e^- + \text{C}_2\text{H}_6 \rightarrow \text{C}_2\text{H}_4^+ + \text{H}_2 + 2e^-$	39
dissociation	$e^- + \text{C}_2\text{H}_6 \rightarrow \text{C}_2\text{H}_5 + \text{H} + e^-$	22
	C ₃ H ₈	
vibr. exc.	$e^- + \text{C}_3\text{H}_8 \rightarrow \text{C}_3\text{H}_8^* + e^-$ (2)	21
dissociation	$e^- + \text{C}_3\text{H}_8 \rightarrow \text{C}_2\text{H}_4 + \text{CH}_4 + e^-$	22
	C ₂ H ₄	
vibr. exc.	$e^- + \text{C}_2\text{H}_4 \rightarrow \text{C}_2\text{H}_4^* + e^-$ (2)	21
ionization	$e^- + \text{C}_2\text{H}_4 \rightarrow \text{C}_2\text{H}_4^+ + 2e^-$	21
dissociation	$e^- + \text{C}_2\text{H}_4 \rightarrow \text{C}_2\text{H}_2 + 2\text{H} + e^-$	21
	C ₂ H ₂	
vibr. exc.	$e^- + \text{C}_2\text{H}_2 \rightarrow \text{C}_2\text{H}_2^* + e^-$ (3)	21
ionization	$e^- + \text{C}_2\text{H}_2 \rightarrow \text{C}_2\text{H}_2^+ + 2e^-$	21

tion in the model. The references of cross sections used in the model for the various reactions are also indicated in Table II. For a methane plasma, a lot of information about the cross sections is known from the literature.^{20,21} In order to obtain a detailed description of the different species in the plasma, “partial” cross sections were used in the model instead of the total cross sections. However, for the following electron reactions, no information about the corresponding cross sections could be obtained:



Therefore, the following approximations are made. For reactions 1 and 2, the total dissociation cross section of C₂H₆²² is used, hence no other dissociation channel is considered. For reactions 3 and 4, the total ionization cross sections of C₂H₄ and C₂H₂ were used (hence, assuming that C₂H₄⁺ and C₂H₂⁺ are the only ionization products). It is mentioned in the literature^{13,23} that reaction 5 is also very important, but no

TABLE III. Ion–neutral reactions taken into account in the model.

Ion–neutral reactions	Reaction rate coefficient (m ³ /s)	Ref.
CH ₄ ⁺ + CH ₄ → CH ₅ ⁺ + CH ₃	1.5 × 10 ⁻¹⁵	8
CH ₃ ⁺ + CH ₄ → C ₂ H ₅ ⁺ + H ₂	1.2 × 10 ⁻¹⁵	8
CH ₅ ⁺ + C ₂ H ₆ → C ₂ H ₅ ⁺ CH ₄ + H ₂	5.0 × 10 ⁻¹⁶	8
H ₂ + H ₂ ⁺ → H ₃ ⁺ + H	2.5 × 10 ⁻¹⁵	25
H ₃ ⁺ + CH ₄ → CH ₅ ⁺ + H ₂	1.6 × 10 ⁻¹⁵	25
H ₃ ⁺ + C ₂ H ₆ → C ₂ H ₅ ⁺ + 2H ₂	2.0 × 10 ⁻¹⁵	25
H ₃ ⁺ + C ₂ H ₄ → C ₂ H ₅ ⁺ + H ₂	1.9 × 10 ⁻¹⁵	25

information about this cross section was found. Therefore, we used a cross section based on the combination of two excitation cross sections.²¹ This is assumed to be a good approximation because it is stated^{18,19} that all excited states of the smaller molecules (CH₄, SiH₄, and Si₂H₆) lead to dissociation. Moreover, it will be demonstrated in Sec. III that this approximation gives results comparable with data found in the literature. Finally, the cross sections of the momentum transfer reactions of the background neutrals, necessary for the solution of the Boltzmann equation, are taken from Ref. 24 for H₂, and from Ref. 20 for the hydrocarbon molecules (CH₄, C₂H₂, C₂H₄, C₂H₆, C₃H₈). These cross sections are not mentioned explicitly in Table II.

2. Ion reactions included in the model

Seven ion–neutral reactions have been included in the model. An overview of these reactions, as well as the reaction rate coefficients can be found in Table III. The first three reactions are taken from Ref. 8, whereas the reactions involving H₃⁺ ions are adopted from Ref. 25. Although some more ion–neutral reactions have been taken into account in the methane model described in Ref. 8, it is found from our calculations (see Sec. III) that the present plasma model with seven ion–neutral reactions gives results comparable with (experimental and calculated) data found in the literature for a wide range of process parameters (pressure, gas inlet flow, power).

3. Neutral–neutral reactions incorporated in the model

In Table IV, an overview is given of the neutral–neutral reactions included in the plasma model. Tachibana *et al.*⁶ described a plasma model with 23 neutral–neutral reactions. We considered only the 12 most important neutral–neutral reactions in order to keep the computational effort low. It can be found from Ref. 6 that a CH₄ molecule reacts with a CH₂ radical to form the excited molecule C₂H₆^{*}, which dissociates rapidly into two CH₃ radicals. Since the dissociation occurs on a short time scale, no excited intermediate state molecules are taken into account in our model. The same applies for some other neutral–neutral reactions. The neutral–neutral reactions where an intermediate excited state was formed (although the latter was not taken into account in the model) are indicated with an a in Table IV.

TABLE IV. Neutral–neutral reactions incorporated in the model.

Neutral–neutral reactions	Reaction rate coefficient (m ³ /s)	Ref.
CH ₃ + CH ₃ → C ₂ H ₆	3.7 × 10 ⁻¹⁷	8
CH ₃ + H → CH ₄	7.0 × 10 ⁻¹⁸	8
C ₂ H ₅ + H → CH ₃ + CH ₃	6.0 × 10 ⁻¹⁷	8
C ₂ H ₅ + CH ₃ → C ₃ H ₈	4.2 × 10 ⁻¹⁸	8
CH ₂ + H → CH + H ₂	2.7 × 10 ⁻¹⁶	8
CH + CH ₄ → C ₂ H ₅	1.0 × 10 ⁻¹⁶	8
CH ₂ + CH ₄ → CH ₃ + CH ₃ ^a	1.7 × 10 ⁻¹⁷	6
CH ₂ + CH ₄ → C ₂ H ₄ + H ₂ ^a	1.7 × 10 ⁻¹⁷	6
CH ₄ + CH → C ₂ H ₄ + H ^a	1.0 × 10 ⁻¹⁶	6
CH ₃ + CH ₂ → C ₂ H ₄ + H	3.3 × 10 ⁻¹⁷	6
C ₂ H ₅ + H → C ₂ H ₄ + H ₂	3.0 × 10 ⁻¹⁸	6
CH ₂ + CH ₂ → C ₂ H ₂ + H ₂	1.1 × 10 ⁻¹⁷	1

^aThese reactions occur over an excited intermediate molecule which is, however, not explicitly taken into account.

4. Transport coefficients

For all the species described in the model, the diffusion coefficients and the mobility coefficients (only for the ions) have to be calculated. For the neutral species (radicals and background neutrals), the diffusion coefficients D_{ij} (m²/s) of the neutral species j in each of the background gases i (CH₄, H₂, C₂H₆, C₃H₈, C₂H₄, C₂H₂) are obtained using the following expression:¹⁹

$$D_{ij} = \frac{3k_b T_{\text{gas}} \sqrt{4\pi k_b T_{\text{gas}} / 2\mu_{ij}}}{16p_{\text{tot}} \pi \sigma_{ij}^2 \Omega_D(\Psi)},$$

where k_b is the Boltzmann constant, T_{gas} stands for the gas temperature of the neutrals which is assumed here to be 400 K. The total pressure is given by p_{tot} (Pa). The reduced mass μ_{ij} is given by $m_i m_j / (m_i + m_j)$. σ_{ij} is the binary collision diameter and Ψ is the dimensionless temperature. The calculation of σ_{ij} and Ψ requires the Lennard–Jones parameters σ (Å) and ϵ (K) for every species. The binary collision diameter σ_{ij} is given by $(\sigma_i + \sigma_j) / 2$, and the dimensionless temperature Ψ equals $T_{\text{gas}} / \epsilon_{ij}$ (with $\epsilon_{ij} = (\epsilon_i \epsilon_j)^{0.5}$). The dimensionless temperature is necessary for the calculation of the dimensionless diffusion collision integral Ω_D , which is given by¹⁹

$$\Omega_D = \frac{A}{\Psi^B} + \frac{C}{e^{D\Psi}} + \frac{E}{e^{F\Psi}} + \frac{G}{e^{H\Psi}},$$

where A, B, C, D, E, F, G , and H are parameters obtained from Ref. 19 ($A = 1.06, B = 0.16, C = 0.19, D = 0.48, E = 1.04, F = 1.53, G = 1.76$, and $H = 3.89$). The Lennard–Jones parameters were found for most of the neutrals (CH₄, C₂H₆, C₃H₈, H₂, C₂H₄, C₂H₂) and for some radicals (H, CH) in Ref. 26. For the other species (radicals and ions), these parameters were calculated by linear interpolation. For example, the Lennard–Jones parameters for the radicals CH₂ and CH₃ were obtained by linear interpolation (from the data for CH and CH₄) using the following formulas:²⁷

$$\sigma_{\text{CH}_x} = \sigma_{\text{CH}} + \frac{x-1}{3} (\sigma_{\text{CH}_4} - \sigma_{\text{CH}}),$$

TABLE V. Lennard–Jones parameters and polarizabilities of all species described in the model.

Species	σ_j (Å)	ϵ_j (K)	α (Å ³)
CH ₄	3.758 ^a	148.6 ^a	2.6
CH ₃	3.620	121.6	
CH ₂	3.491	95.2	
H	2.708 ^a	37.0 ^a	
C ₂ H ₆	4.443 ^a	215.7 ^a	4.47
C ₂ H ₅	4.443	215.7	
C ₃ H ₈	5.118	237.1	6.33
CH	3.370 ^a	68.6 ^a	
H ₂	2.827 ^a	59.7 ^a	0.819
C ₂ H ₄	4.163 ^a	224.7 ^a	4.22
C ₂ H ₂	4.033 ^a	231.8 ^a	3.49

^aValues taken from Ref. 26, all other values are calculated by interpolation.

$$\epsilon_{\text{CH}_x} = \epsilon_{\text{CH}} + \frac{x+1}{3} (\epsilon_{\text{CH}_4} - \epsilon_{\text{CH}}),$$

where x has the value of 2 and 3 for CH₂ and CH₃, respectively. For C₂H₅, the Lennard–Jones parameters could not be obtained by linear interpolation [due to the difference in molecule configuration between C₂H₆ (sp^3) and C₂H₄ (sp^2)]; therefore we used the values of C₂H₆. An overview of the Lennard–Jones parameters of the species can be found in Table V.

Finally, the diffusion coefficient D_j of the species j in the entire gas mixture (the sum of all the background gases i) is obtained from the different D_{ij} values using²⁸

$$\frac{P_{\text{tot}}}{D_j} = \sum_{i=\text{background}} \frac{P_i}{D_{ij}},$$

with p_{tot} the total pressure and p_i the partial pressure of the background gas i . The ion mobility coefficients μ_j (m²/Vs) of the ions in the gas mixture can be calculated in a similar way as the diffusion coefficients for the neutral species. First, the ion mobility coefficient $\mu_{i,j}$ of an ion j in each of the background gases i is calculated using²⁸

$$\mu_{i,j} = 0.514 \frac{T_{\text{gas}}}{P_{\text{tot}} \sqrt{\mu_{ij} \alpha_i}}.$$

The reduced mass μ_{ij} is here given in amu, while α_i (Å³) is the polarizability of the background gas i . All other parameters used in the above equation have been defined before. The polarizabilities are taken from Ref. 29 and are also presented in Table V. Finally, the ion diffusion coefficient D_j of an ion j in the total gas mixture can be obtained using the Einstein relation

$$D_j = \frac{k_b T_{\text{ion}}}{e} \mu_j,$$

with T_{ion} the ion temperature (which is assumed to be equal to the gas temperature) and μ_j the mobility coefficient of the ion in the gas mixture.

5. Boundary conditions

The boundary conditions for the different species are incorporated in the fluid model by means of a “sticking model”,¹⁴ so that some preliminary information can also be

TABLE VI. Discharge parameters for which the calculations are performed. The power, CH₄ and H₂ gas flow, and the pressure are varied in the range indicated to investigate their effect on the calculated results.

Settings	Value
rf frequency	13.56 MHz
electrode spacing	0.03 m
electrode radius	0.1 m
gas temperature	400 K
power	15–80 W
CH ₄ gas flow	5–25 sccm
H ₂ gas flow	0–10 sccm
pressure	0.14–0.5 Torr

obtained about the growth of the layer. In this model, the radicals and the ions react with the surface, while the non-radical neutral molecules do not influence the growth of the layer. It is assumed that all the ions have a sticking coefficient of 1.⁴ The radicals taken into account for the film growth in the model are CH₃, CH₂, and C₂H₅, with a sticking coefficient of 0.01,^{30,31} 0.025,³² and 0.01,^{7,33} respectively. When a radical sticks to the substrate, not all atomic hydrogen is incorporated in the layer. The amount of hydrogen incorporated into the layer is set to 30%, the other amount of atomic hydrogen flows back into the plasma as molecular hydrogen gas. While the radicals CH₃, CH₂, and C₂H₅ contribute to the film growth, the H radicals etch the layer to form volatile CH₄ molecules.^{4,31} Because no exact data are known for the etching process, this rate has been fitted to obtain a growth rate that corresponds well to the values found experimentally. Using this constant fitting parameter, the calculated deposition rate corresponds well with the experimental deposition rate² in the power range of 20–120 W.

III. RESULTS AND DISCUSSION

Typical results of the fluid model are the densities of the various species, the electric field, and the electron density as a function of distance between the electrodes and as a function of time in the rf cycle. Moreover, information is obtained about the fluxes of the different species towards the electrodes, and about the plasma characteristics (rf voltage, plasma potential, ohmic heating of the electrons, and various ions). In this work, we will concentrate on the calculated density profiles of the various plasma species between the electrodes. The effect of power, gas mixture (CH₄/H₂), gas inlet flow, and pressure will be investigated. The parameter ranges for which the calculations are performed are given in Table VI.

A. Calculated densities of the plasma species versus distance in the plasma

Figure 1 illustrates the calculated densities of the non-radical neutral molecules, the radicals and the ions considered in the model at 0.14 Torr, 25 W, 13.56 MHz, and 20 sccm CH₄ inlet. The densities of the background neutrals (CH₄, H₂, C₂H₆, C₂H₄, C₂H₂, C₃H₈) are homogeneously distributed between the electrodes. It can be seen that the higher order hydrocarbon molecules (C₂H₆, C₂H₄, C₂H₂, C₃H₈),

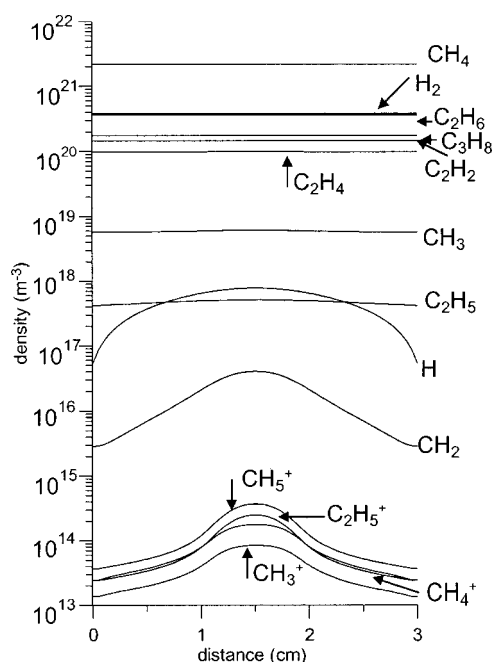


FIG. 1. Calculated densities of the nonradical neutrals, radicals, and ions as a function of distance from the electrode at 0.14 Torr, 25 W, 13.56 MHz, and 20 sccm inlet methane (no H₂ inlet).

which are formed by the neutral–neutral reactions mentioned in Table IV, are not negligible compared to CH₄ (i.e., only one order of magnitude lower density). The presence of these higher order hydrocarbon molecules at high densities in a methane plasma differs from a silane plasma, where only SiH₄, H₂, and Si₂H₆ are present at such high densities.¹⁴ By means of mass spectrometry, Dagele *et al.*¹² measured the partial pressures of these background neutrals in a rf methane plasma. These experiments have been carried out under somewhat different experimental conditions (0.03 Torr, methane gas flow varying between 2.4 and 10.4 sccm) than the parameters used in our theoretical calculations. However, the same tendency (i.e., the presence of the higher order hydrocarbon molecules in the plasma) was found. It should be mentioned that the influence of the gas inlet and the background pressure on the relative abundancies of the species densities is rather small (see Figs. 6 and 7 below), so that the comparison of the experimental data with our calculated result is justified.

Further, it follows from Fig. 1 that the most important radical in the plasma is found to be CH₃ with a density of about $5 \times 10^{18} \text{ m}^{-3}$ (more or less constant throughout the plasma). This is in agreement with the experimental density of CH₃ (about 10^{18} m^{-3} at 0.123 Torr and 10 W) obtained by Sugai *et al.*³⁴ and the density calculated by Bera *et al.*¹¹ (about 10^{18} m^{-3} at 0.123 Torr). The calculated CH₂ radical density (in the order of 10^{16} m^{-3}) also agrees with the results measured by Sugai *et al.*³⁴ [i.e., also in the order of 10^{16} m^{-3} (at 0.123 Torr and 10 W)].

The calculated density of the C₂H₂ molecules (about 10^{20} m^{-3}) is also in good agreement with the C₂H₂ density (10^{20} m^{-3} at 0.2 Torr and 500 W) measured by Wormhoudt.³⁵ Although the power used in the experiment (500 W) is much

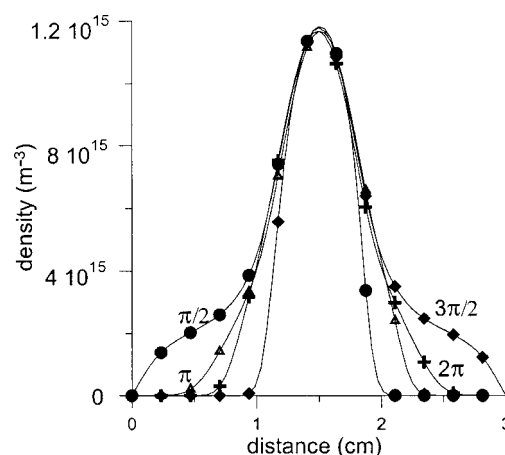


FIG. 2. Calculated electron density at four phases of the rf cycle [$\pi/2$ (●), π (▲), $3\pi/2$ (◆), and 2π (+)]. The discharge parameters are kept the same as in Fig. 1.

higher than the power assumed in the calculation (25 W), the density values are the same. This is, however, logical because our calculations predict that the densities of the nonradical molecules do not vary significantly with power (see Fig. 3 below). In general, the densities calculated with our model also correspond with the results obtained by Tachibana *et al.*,⁶ who calculated the densities of a variety of species in a wide range of power (10^{-1} – 10^3 W) at 0.22 Torr. However, some differences in species densities can be seen. This can be explained by the fact that different models include different reactions which affect the results of the model to a certain extent.

Finally, Fig. 1 also presents the densities of the ions in the plasma. Only the densities of the most important ions (CH₅⁺, C₂H₅⁺, CH₄⁺, and CH₃⁺) are shown; the densities of the other ions considered in the model (C₂H₄⁺, C₂H₂⁺, H₂⁺, and H₃⁺) are not given. Note that the C₂H₄⁺ and C₂H₂⁺ densities actually represent the group of ions (i.e., for C₂H₄: C₂H₄⁺, C₂H₃⁺, C₂H₂⁺, CH₃⁺, CH₂⁺) formed in the ionization reactions with C₂H₄ and C₂H₂, respectively. This follows from the fact that we used the total ionization cross sections for these two reactions. It should be noted that for the ion density the time averaged value is given because the ion density changes slightly with time in the sheath zone. The densities of the radicals and neutrals, on the other hand, do not change as a function of time.

The electron density is found to be in the order of 10^{15} electrons/m³. In Fig. 2, the electron density is shown at four phases ($\pi/2$, π , $3\pi/2$, 2π) of the rf cycle. It can be seen that the electron density changes strongly as a function of time in the sheath zone, whereas the density in the bulk plasma stays nearly constant.

B. Effect of varying power

We have carried out six simulations in the power range between 15 and 100 W, while all other plasma parameters were kept constant (see Sec. III A). The densities (in the middle of the plasma) of the most important nonradical neutral background molecules, the electrons, the ions, and the radicals are plotted in Fig. 3 as a function of power. From

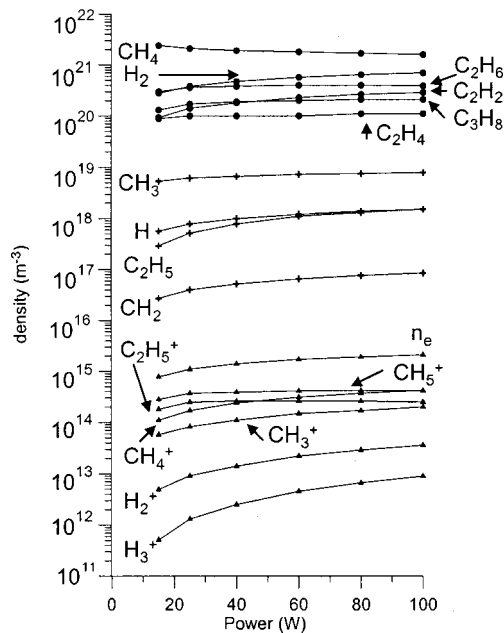


FIG. 3. Calculated densities of the nonradical neutrals (●), radicals (+), ions, and electrons (▲) as a function of power going into the plasma. The other parameters are kept the same as in Fig. 1.

this figure, it can be seen that the CH_4 density decreases somewhat with increasing power, whereas all the other plasma species densities (nonradical neutrals, radicals, ions, and electrons) are slightly increasing. The tendencies in our results are in agreement with the results found by Tachibana *et al.*,⁶ who performed simulations in a much wider range of power (10^{-1} – 10^3 W) for a similar discharge pressure (0.22 Torr). Good agreement was also reached between our results and the calculated densities of the radicals and the neutrals found by Rhallabi and Catherine⁹ at 0.08 Torr and by Gogolides *et al.*¹ at 0.14 Torr.

The most important ion at low power (15 W) is clearly found to be CH_5^+ , while at highest power (100 W) CH_4^+ becomes equally important. The electron density increases from about $8 \times 10^{14} \text{ m}^{-3}$ at 15 W to about $2 \times 10^{15} \text{ m}^{-3}$ at 100 W.

Dekempeneer *et al.*² have measured, by use of mass spectrometry, the so-called conversion factor of CH_4 under varying power conditions (0–120 W), at different pressures. The conversion factor *cf* was defined by²

$$cf = 1 - \frac{I}{I_0},$$

where I and I_0 are the CH_4 densities in the plasma when the discharge was on and off, respectively. It is worthwhile to mention that although this factor was called “dissociation degree” in Ref. 2, we prefer to call it *conversion factor*, because the term gives information about how many methane molecules have reacted, not only due to dissociation but also due to ionization and neutral–neutral reactions. A comparison between the experimental and calculated values for the conversion factor as a function of power, at the same plasma conditions as the experiment (20 Pa, 8 sccm CH_4 , and 4 sccm H_2), is given in Fig. 4. It can be seen that in both

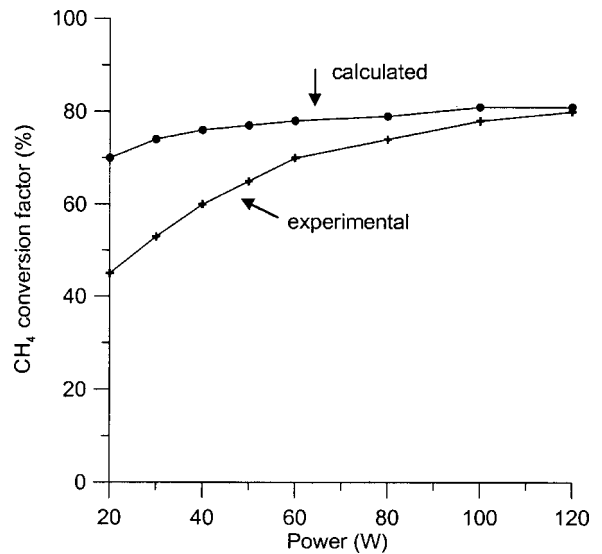


FIG. 4. Comparison between the experimental and calculated methane conversion factor as a function of power.

cases the conversion factor increases with rising power. At higher power, a good agreement was reached, whereas at low power the agreement is less satisfactory. It should be noted that the power values used in the model correspond to the powers that are effectively put into the plasma. It is generally known that not all the power from the rf generator effectively goes into the plasma, but the exact percentage is not known. We assumed that the *power going into the plasma is 50% of the generator power*, in analogy to Ref. 14. Hence, it is very difficult to compare the calculated and experimental results in absolute terms, but the general trends appear to be already in satisfactory agreement.

C. Effect of varying gas flow mixture

To investigate the effect of the gas flow mixture, the latter was changed from 20 sccm pure CH_4 to a mixture of 10 sccm CH_4 and 10 sccm H_2 (with intervals of 2 sccm). All the simulations were carried out with a total gas flow of 20 sccm while all other plasma parameters were kept constant (see Sec. III A). The results of these simulations can be found in Fig. 5 for the densities of the neutral molecules, the radicals, the ions, and the electrons. The densities of the nonradical neutrals increase in the same linear way with rising CH_4 sccm gas flow, except for the H_2 density, which is logical because the H_2 gas flow decreases. The densities of the radicals appear not to be significantly influenced by the change of CH_4/H_2 gas flow mixture, except for the density of CH_3 , which increases slightly with increasing CH_4 gas flow. As far as the ions are concerned, the H_2^+ and H_3^+ ion densities decrease more drastically with rising CH_4 gas flow (and hence decreasing H_2 gas flow) than the CH_4^+ and CH_3^+ densities, which also decrease to a certain extent. The densities of the CH_5^+ and C_2H_5^+ ions, on the other hand, appear to increase with rising CH_4 gas mixture. This can be explained by the ion–neutral reactions which create mainly CH_5^+ and C_2H_5^+ at rising CH_4 gas flow.

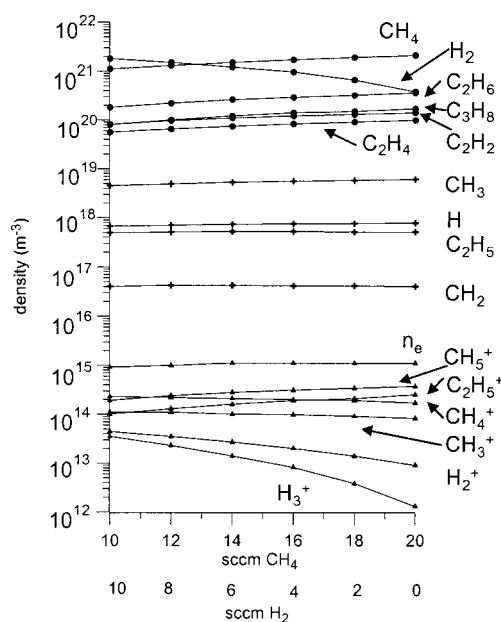


FIG. 5. Calculated densities of the nonradical neutrals (●), radicals (+), ions, and electrons (▲) as a function of CH₄ and H₂ gas flow mixture. The total gas flow is kept constant at 20 sccm; the CH₄ gas flow varies between 10 and 20 sccm, whereas the H₂ gas flow varies between 0 and 10 sccm. The other parameters are kept the same as in Fig. 1.

D. Effect of varying total gas flow

The calculated densities of the nonradical neutral molecules, the radicals, the ions, and the electrons as a function of increasing total gas flow (i.e., 5–25 sccm CH₄, no H₂) is given in Fig. 6. All other plasma parameters were kept constant (see Sec. III A). The CH₄ density increases with rising CH₄ flux, which is logical. The densities of the other species remain more or less constant, or decrease slightly. As a con-

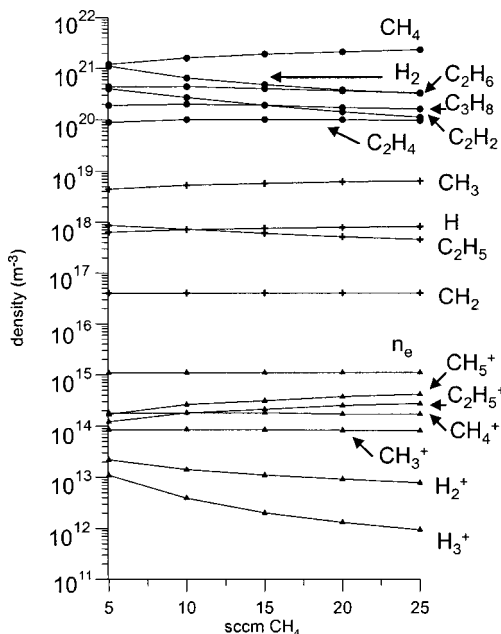


FIG. 6. Calculated densities of the nonradical neutrals (●), radicals (+), ions, and electrons (▲) as a function of CH₄ sccm (no H₂ inlet). The other parameters are kept the same as in Fig. 1.

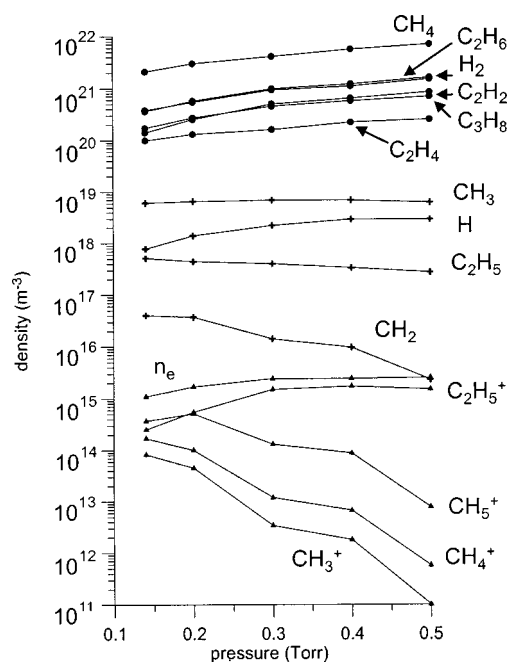


FIG. 7. Calculated densities of the nonradical neutrals (●), radicals (+), ions, and electrons (▲) as a function of gas pressure. The other parameters are kept the same as in Fig. 1.

sequence of the constant pressure, the residence time of the different species decreases when rising the inlet flow of CH₄. When the residence time of the species decreases, the molecules are pumped out of the reactor more rapidly. This implies that less reactions (neutral–neutral and ion–neutral reactions) can occur between these molecules, so less H₂ is formed. (because H₂ is the major reaction product in most of the reactions, see Tables III and IV). This explains why the H₂ density decreases when more CH₄ is introduced in the reactor at constant pressure. The densities of the radicals and of the hydrocarbon ions (CH₅⁺, C₂H₅⁺, CH₄⁺, CH₃⁺) are not heavily influenced by changing the CH₄ gasflow. The H₂⁺ and the H₃⁺ ion densities drop more clearly with rising CH₄ gas flow, because less H₂ is present in the plasma (see above) and because H₂⁺ reacts further to H₃⁺, which afterwards reacts to CH₅⁺ or C₂H₅⁺ by ion–neutral reactions.

E. Effect of varying pressure

In order to study the effect of gas pressure, five simulations were carried out in the range varying from 0.14 to 0.5 Torr. The densities of the nonradical neutrals, the radicals, the ions, and the electrons are plotted as a function of pressure in Fig. 7. Note that for each simulation at a certain pressure, the transport coefficients have to be recalculated from the formulas described in Sec. II B 4. The densities of the nonradical neutrals increase slightly for all species as a function of pressure. The densities of the radicals do not vary significantly with pressure (except for CH₂, which decreases significantly at rising pressures). The C₂H₅⁺ ion density increases to the same extent with rising pressure as the nonradical neutrals, while all the other ion densities (CH₅⁺, CH₄⁺, CH₃⁺) drop drastically. This can be explained by the fact that at higher pressures ion–neutral reactions become more im-

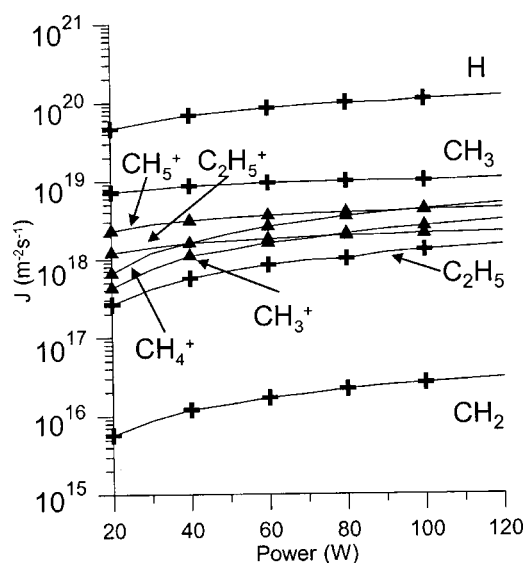


FIG. 8. Calculated radical (CH_3 , CH_2 , C_2H_5 , H) and ion (CH_4^+ , CH_3^+ , CH_5^+ , C_2H_5^+) fluxes towards the electrodes as a function of power. The other parameters are kept the same as in Fig. 1.

portant. As can be seen from Table III, in most of the ion-neutral reactions, CH_5^+ and C_2H_5^+ are formed. CH_5^+ can also further react to C_2H_5^+ , hence this explains why C_2H_5^+ becomes the major ion at higher pressures.

F. Information of the fluxes towards the electrodes

As mentioned in Sec. II B 5, the growth of the layer depends on the fluxes of the radical and ionic species towards the electrodes. In Fig. 8, the fluxes ($\text{m}^{-2} \text{s}^{-1}$) of the radicals (CH_3 , CH_2 , C_2H_5 , H) and ions (CH_4^+ , CH_3^+ , CH_5^+ , C_2H_5^+) are presented as a function of power. The other plasma parameters were kept constant (see Sec. III A). It can be seen from Fig. 8 that all the fluxes (except CH_5^+ and C_2H_5^+) increase slightly as a function of power. Because no bias voltage can be applied in the 1D model, the fluxes towards both electrodes (powdered and grounded electrode) are the same. Note that the H flux contributes to the erosion of the layer, while the other fluxes determine the growth of the layer (see Sec. II B 5).

IV. CONCLUSION

A 1D fluid model for a methane capacitively coupled rf plasma has been presented. The fluid model, coupled with the Boltzmann equation to calculate the EEDF predicts the densities of the various plasma species (neutrals, radicals, ions). This has been illustrated over a wide range of plasma parameters (power, gas flow, gas flow mixture, pressure). To validate our model, we compared our calculated results with experimental and calculated data available from the literature. From this comparison it can be concluded that the developed methane model (consisting of 20 species) is able to predict the different species densities quite well. It is found that also the higher hydrocarbon molecules (C_2H_6 , C_2H_4 , C_2H_2 , C_3H_8) are present in the methane discharge in contrast to a silane plasma. The main radical is found to be CH_3 , while the most important ions are found to be C_2H_5^+ , CH_5^+ ,

CH_4^+ , and CH_3^+ . Although the densities of H_2^+ and H_3^+ are found to be rather low, they play an important role in the ion-neutral reactions to form mainly the ions CH_5^+ and C_2H_5^+ . In total, 14 vibrational excitation reactions have been taken into account with the different background neutrals, in order to obtain a more accurate EEDF. It should be noted that the results in this article are restricted to the alpha regime, hence no secondary electrons are taken into account. In the future, we plan to extend the methane plasma model to a 2D geometry, in order to obtain information about the uniformity of the plasma in the reactor, and about the uniformity of the deposited layer. The present model already gives information about the fluxes of the different species towards the electrodes, however, a detailed deposition model has not yet been included.

ACKNOWLEDGMENTS

The authors acknowledge financial support from the Vlaamse Instelling voor Technologisch onderzoek (VITO), the Federal Services for Scientific, Technical and Cultural Affairs (DWTC/SSTC) of the Prime Ministers Office through IUAP 4 (conv. P4/10), a New Research Initiative (UIA), and the Flemish Fund for Scientific Research (FWO). This research is also sponsored by NATO's Scientific Affairs Division in the framework of the Science for Peace program. Finally, they wish to thank A. V. Phelps and H. Tawara for their useful information about the cross sections used in the model.

- ¹E. Gogolides, D. Mary, A. Rhaballi, and G. Turban, *Jpn. J. Appl. Phys., Part 1* **34**, 261 (1995).
- ²E. Dekempeneer, J. Smeets, J. Meneve, L. Eersels, and R. Jacobs, *Thin Solid Films* **241**, 269 (1994).
- ³D. S. Patil, K. Ramachandran, N. Venkatramani, M. Pandey, S. Venkatswaran, and R. D. Cunha, *J. Alloys Compd.* **278**, 130 (1998).
- ⁴A. Von Keudell and W. Möller, *J. Appl. Phys.* **75**, 7718 (1994).
- ⁵A. Vanhulsel, J. P. Celis, E. Dekempeneer, J. Meneve, J. Smeets, and K. Vercammen, *Diamond Relat. Mater.* **8**, 1193 (1999).
- ⁶K. Tachibana, M. Nishida, H. Harima, and Y. Urano, *J. Phys. D: Appl. Phys.* **17**, 1727 (1984).
- ⁷N. Mutsukura, S. Inoue, and Y. Machi, *J. Appl. Phys.* **72**, 43 (1992).
- ⁸L. E. Kline, W. D. Partlow, and W. E. Bies, *J. Appl. Phys.* **65**, 70 (1988).
- ⁹A. Rhallabi and Y. Catherine, *IEEE Trans. Plasma Sci.* **19**, 270 (1991).
- ¹⁰C. Cavalotti, M. Masi, and S. Carrà, *J. Electrochem. Soc.* **145**, 4332 (1998).
- ¹¹K. Bera, B. Farouk, and Y. H. Lee, *J. Electrochem. Soc.* **146**, 3264 (1999).
- ¹²D. J. Dagel, C. M. Mallouris, and J. R. Doyle, *J. Appl. Phys.* **79**, 8735 (1996).
- ¹³M. Masi, C. Cavalotti, and S. Carrà, *Chem. Eng. Sci.* **53**, 3875 (1998).
- ¹⁴G. J. Nienhuis, W. J. Goedheer, E. A. G. Hamers, W. G. J. H. M. Van Sark, and J. Bezemer, *J. Appl. Phys.* **82**, 2060 (1997).
- ¹⁵G. J. Nienhuis, Ph.D. thesis, Utrecht University 1998.
- ¹⁶G. J. Nienhuis and W. Goedheer, *Plasma Sources Sci. Technol.* **8**, 295 (1999).
- ¹⁷G. Smolinski and M. J. Vasile, *Int. J. Mass Spectrom. Ion Phys.* **16**, 137 (1975).
- ¹⁸W. L. Morgan, *Plasma Chem. Plasma Process.* **12**, 477 (1992).
- ¹⁹J. Perin, O. Leroy, and M. C. Bordage, *Contrib. Plasma Phys.* **36**, 3 (1996).
- ²⁰H. Tawara, Y. Itikawa, H. Nishimura, H. Tanaka, and Y. Nakamura, Research Report NIFS-DATA6, ISSN 0915-6364, Nagano, Japan, 1990.
- ²¹H. Tawara, in *Electron Collision Processes Involving Hydrocarbons*, Atomic and Molecular Processes in Fusion Edge Plasmas, edited by R. K. Janev (Plenum, New York, 1995), Chap. 16.
- ²²F. Winters, *Chem. Phys.* **36**, 353 (1979).
- ²³R. Gordon and P. Ausloos, *J. Chem. Phys.* **47**, 1977 (1967).

- ²⁴L. Ehrhardt, L. Langhans, F. Linder, and H. S. Taylor, *Phys. Rev.* **173**, 222 (1968).
- ²⁵J. A. Burt, J. L. Dunn, M. J. McEwan, M. M. Sutton, A. E. Roche, and H. I. Schiff, *J. Chem. Phys.* **52**, 6062 (1970).
- ²⁶R. H. Svela, NASA Report, NASA-TR-132 (1962).
- ²⁷M. E. Coltrin, R. J. Kee, and J. A. Miller, *J. Electrochem. Soc.* **133**, 1206 (1986).
- ²⁸E. W. Mc Daniel and E. A. Mason, *The Mobility and Diffusion of Ions in Gases* (Wiley, New York, 1973).
- ²⁹C. J. F. Böttcher and P. Bordewijk, *Theory of Electric Polarisation* (Elsevier Scientific, Amsterdam, 1978), Vol. 2.
- ³⁰C. Hopf, K. Letourneur, W. Jacob, T. Schwarz-Selinger, and A. Von Keudell, *Appl. Phys. Lett.* **74**, 3800 (1999).
- ³¹A. Von Keudell, T. Schwarz-Selinger, M. Meier, and W. Jacob, *Appl. Phys. Lett.* **76**, 676 (2000).
- ³²H. Kojima, H. Toyoda, and H. Sugai, *Appl. Phys. Lett.* **55**, 1292 (1989).
- ³³C. Hopf, T. Schwarz-Selinger, W. Jacob, and A. Von Keudell, *J. Appl. Phys.* **87**, 2719 (2000).
- ³⁴H. Sugai, H. Kojima, A. Ishida, and H. Toyoda, *Appl. Phys. Lett.* **56**, 2616 (1990).
- ³⁵J. Wormhoudt, *J. Vac. Sci. Technol. A* **8**, 1722 (1990).
- ³⁶T. Nakanu, H. Toyoda, and H. Sugai, *Jpn. J. Appl. Phys., Part 1* **30**, 2912 (1991).
- ³⁷A. G. Engelhardt and A. V. Phelps, *Phys. Rev.* **131**, 2115 (1963).
- ³⁸H. Tawara and T. Kato, *At. Data Nucl. Data Tables* **36**, 167 (1987).
- ³⁹H. Chatman, D. Hils, R. Robertson, and A. Gallagher, *J. Chem. Phys.* **81**, 1770 (1984).